THE INFLUENCE OF STEEL SLAG AND NANOCLAY ADDITIVES ON THE MECHANICAL AND DURABILITY PERFORMANCE OF UNSATURATED POLYESTER GYPSUM BASED COMPOSITES

Ahmad Mousa

Department of Materials Engineering, Faculty of Engineering
Al-Balqa Applied University, Salt 19117, Jordan, mousa@rocketmail.com, mousa1@bau.edu.jo (A.M.).

Received 07 March 2026
Accepted 22 April 2026
DOI: 10.59957/jctm.v61.i5.2026.10

ABSTRACT

The current investigation examines the development and characterization of gypsum-based hybrids incorporating industrial steel slag, organo-modified nanoclay (Nanofil-15), and an unsaturated polyester (UP) resin. The formulations were designed to compare a conventional water-resistant system with UP-bound system. The fabricated samples were evaluated in terms of specific impact strength (Si), flexural performance, water absorption, and direct flame resistance. Microstructural analysis by scanning electron microscopy (SEM) was correlated with porosity (Vv) to clarify the relationship between packing efficiency and interfacial voids. The UP-bound gypsum (UPG) composite exhibited a substantial increase in impact resistance compared to the water-bound system primarily due to coordination interaction between the UP-carbonyl groups and the surface Ca^{2+} and Al^{3+} cations, which strengthen the interface between the amorphous slag and crystalline gypsum phases. Incorporation nanoclay and stearic acid-modified slag (LS) further improved mechanical performance by promoting crack-deflection and interfacial micro-lubrication. The UP resin drastically reduced water absorption (< 1.0 %) by forming a hydrophobic shield around the mineral. Furthermore, slag additions which is rich in Fe_2O_3 and Al_2O_3 reduced the mass loss rate (MLR) by acting as an inorganic heat sink. These findings highlight the synergistic potential of polymer-mediated coordination to convert waste material into a durable, high-strength construction material.

Keywords: slag, unsaturated polyester, organo nanoclay, coordination bond, amorphous-crystalline synergy, impact strength, fire resistance, porosity.

INTRODUCTION

Gypsum is a widely used construction material known for its versatility, ease of shaping, and relatively low energy compared with binders such as cement or lime [1 - 5]. However, its application is limited by its intrinsic brittleness and low water resistance. Improper disposal of gypsum waste from construction and renovation activities can pose environmental challenges [6 - 9]. Industrial by-products such as mine tailings, fly ash, and steel slag pose similar environmental concerns when disposed of in large quantities [10 - 14]. Steel slag has gained attention due to its chemical reactivity and its successful incorporation into various polymer matrices in earlier studies [15 - 19]. Reintegrating such industrial by-products into gypsum-based materials offers two key advantages: reducing environmental impact and enhancing the mechanical and durability performance of the composites. Depending on the desired properties, these improvements can further be tailored using appropriate organic and inorganic fillers. In this work, unsaturated polyester (UP) resin is used as an organic binder to reinforce the gypsum matrix, while steel slag and organo-modified layered nanoclay are incorporated as inorganic additives to enhance structural integrity and durability. This investigation has two main objectives: (1) to develop gypsum-based systems with a various filler with and without an organic binder, and (2) to evaluate the effect of these additions on mechanical performance, water absorption, and fire resistance. Unlike traditional mineral composites that depend largely on mechanical interlocking, the materials here function as polymer-mineral hybrids. This is due to strong coordinative interaction between the carbonyl

group of the UP resin and the Ca^{2+} and Al^{3+} ions on the surfaces of both the slag and the gypsum, forming a unified hybrid network that improves energy dissipation and moisture resistance.

EXPERIMENTAL

Materials and reagents

Commercial-grade gypsum powder (Al-Safa Co., Saudi Arabia) and raw Iron Slag (S) was obtained from a local iron manufacturer in Jordan. The gypsum and slag's chemical oxide composition are shown in Table 1. Unsaturated Polyester (UP) resin, Cobalt Naphthenate, and Methyl Ethyl Ketone Peroxide (MEKP), stearic acid all supplied by Intermediate Petrochemicals Industries (IPI, Jordan). organo-layered nanoclay (Nanofil-15, Süd-chemie AG, Germany),

Formula

Table 2. Recipe used to produce the gypsum-based hybrids with and without binder.

Mechanical pretreatment of steel slag

The raw slag lumps were comminute using a roll crusher (Model AF32A). The resulting coarse particles underwent dry ball milling for 16 h at 320 rpm (US Stoneware, OH). The powder was then sieved using an electronic shaker (Retsch AS 200) to a fraction ≤ 250 μm.

Chemical functionalizing of slag

To enhance surface interaction and dispersion, a portion of the slag was treated to produce lubricated slag (LS) by immersing the slag powder in 10 % stearic acid solution in toluene. The mixture was continuously mixed using electrical mixer for 6 h. The mixture was filtered and dried. The chemical functionalization of the steel slag involves a coordination reaction between the COOH of the stearic acid and the surface-active Ca^{2+} and Al^{3+} cations. The expected result is insoluble, monomolecular layer of calcium and aluminium stearates. This transformation converts the polar, hydrophilic oxide surfaces into non-polar, organophilic interfaces at the slag-gypsum boundary.

Sample fabrication (water bound)

The control specimens were prepared through a controlled hydration process. The gypsum raw powder was dry-blended with the steel slag and organo-clay for 5 min. to ensure a homogenous distribution of the inorganic phases. This dry mixture was then gradually added to

Table 1**.** Chemical oxide composition of the raw gypsum and steel slag determined by X-ray fluorescence (XRF) using Shimadzu EDX-800HS.

Material	CaO, %	SO_3, %	SiO_2 (%)	Al_2O_3, %	MgO, %	Fe_2O_3, %
Gypsum	44	41	7	3	2	1.2
Steel Slag	31	-	19	13	-	28

Table 2. Recipe used to produce the gypsum-based hybrids with and without binder.

Symbol	Formulation (parts by weight)	Components
G	75 / 25	Gypsum
GS	75 / 25 / 25	Gypsum + raw steel slag
GN	75 / 25 / 3	Gypsum + organo-nanoclay
GLS	75 / 25 / 25	Gypsum + lubricated slag
UPG	75 / 15 / 10	Gypsum + UP resin control
UPGS	75 / 15 / 25 / 10	Gypsum + slag + UP
UPGN	75 / 15 / 5/ 10	Gypsum + nanoclay + UP
UPGLS	75 / 15 / 25 / 10	Gypsum + lub. slag + UP

deionized water at a standardized water-to-binder (75/25) ratio. The resulting slurry was mechanically agitated to facilitate the dissolution of gypsum and the subsequent nucleation of gypsum crystals. The mixture was cast into Teflon molds and vibrated to eliminate entrapped air. The samples were left to set for 24 h, the specimens were demolded and subjected to thermal conditioning at 40°C until a constant mass was achieved.

Hybrid specimen fabrication (UP bound)

The preparation of the hybrids involved the dispersion of the inorganic additives directly into the organic binder under high-shear mixing, according to the mixing ratio shown in Table 2. Following the addition of the catalyst, the pre-mixed gypsum-water slurry was added to the resin phase. The resulting hybrids were cast in Teflon molds and left to set for 72 h at room temperature. Samples were prepared based on the weight ratios defined in Table 3. The curative system (0.3 % Cobalt and 0.3 % MEKP was added at the last stage of mixing [20, 21]. The process involved dual-curing process.

Impact strength

The impact strength was evaluated using a CEAST impact tester (Model 6545) on unnotched 10 × 3 × 60 mm specimens according to ASTM D-356-88. The hammer energy was 7.5 J at a velocity of 3.0 m s^{-1}. The absorbed energy was converted to impact strength using Eq. (1) and Eq. (2):

$$\text{Impact strength} = \frac{\text{Fracture Energy}}{\text{Cross sectional area}} \quad (1)$$

$$\text{Specific impact strength } (S_i) = \frac{\text{impact strength}}{\text{density}} \quad (2)$$

Flexural stress

Rectangular samples (10 × 3 × 150 mm) were subjected to three-point bending using a HOYTOM universal testing machine (10 kN max load) In accordance with ASTM C39/C39M-16. The breaking load was converted to flexural strength using the following model described in Eq. (3):

$$\sigma = \frac{3.P.L}{2.b.d^2} \quad (3)$$

where: P = applied load, L = support span, b = width, and d = thickness

Density measurement

Rectangular specimens were wrapped in thin paraffin-wax sheets to create a waterproof barrier. After recording the mass and measuring water displacement, the true density was calculated by correcting for the wax volume (Eq. (4)):

$$\rho = \frac{M_s}{V_{total} - (\frac{Mw}{\rho w})} \quad (4)$$

where M_s is specimen dry mass, V_{total} is displaced volume, Mw is wax mass, and ρ_w is the density of wax 0.90 g cm^{-3}.

Water Uptake Percentage

Pre-weighed samples of 3 mm thick were submerged in water at room temperature for 6 h until they reached a constant weight. Weight gain was computed according to the Eq. (5):

$$M\% = (\frac{Final\ weight - Initial\ weight}{initial\ weight}) \times 100 \quad (5)$$

The degree of porosity (Vv) of the samples was calculated as well using the Eq. (6):

$$V_v = \frac{\rho_{exp} - \rho_{th}}{\rho_{th}} \quad (6)$$

ρ_{th} is the theoretical density assuming zero air entrapment, ρ_{exp} is the experimental density.

Fire resistance:

A three-gram rectangular sample was mounted vertically for 30 s. The sample was in direct contact with a torch flame. Following a reweighing of the sample, the mass loss percentage was calculated according to the following model of Eq. (7):

$$\text{Mass Loss\%} = (\frac{\text{Initial mass} - \text{Final mass}}{\text{Initial mass}}) \times 100 \quad (7)$$

The MLR was calculated according to the Eq. (8):

$$MLR = \frac{M_i - M_f}{A.t} \quad (8)$$

M_i - M_f: The actual mass loss in grams (g), A is the surface area of the exposed face and t, is the exposure

time (30 s).

Scanning electron microscopy (SEM)

The fractured surfaces of the impact-tested specimens were coated with a tiny layer of silver to prevent electrostatic charge during examination. This was done using SCD device from BALTEC Company. The samples were magnified using an XL-30 W/TMP electron scanning microscope type from Tokyo, Japan.

RESULTS AND DISCUSSION

Impact strength of gypsum hybrids

The specific strength of gypsum-based hybrids is calculated according to Eq. (1) and (2) respectively, is compared for samples both with and without reinforcements, in Table 3. Note that the pure gypsum, G, exhibited the lowest specific impact strength. This behaviour is linked to the brittle nature of the $CaSO_4.2H_2O$ crystalline structure. Therefore, it lacks mechanisms for plastic deformation. Consequently, the material undergoes catastrophic failure under impact loading. This finding is consistent with established literature regarding the abrupt fractured tendencies of unreinforced gypsum-based systems [22]. The incorporation of raw steel slag yielded a marginal improvement in Si compared to the control as presented in Table 3. This increment suggests a limited degree of stress sharing between the gypsum matrix and the slag fillers. Note that, irrespective that both components share a high calcium oxide specifically, 44 % CaO in gypsum and 31 % in slag as demonstrated by the XRF data shown in Table 1, the interfacial bonding remains relatively weak. This suggests that only mechanical interlock is taking place. This is due to their compatibility is fundamentally governed by the fact that the slag is primarily an amorphous silicate with 19 % SiO_2 as presented in Table 1. This means that it possesses high internal energy, while the gypsum exists as a stable crystalline sulfate with 41 % SO_3 shown in Table 1 as well. Their chemical profiles suggest improved degree of interactions through dissolution-precipitation reactions. However, the smooth, iron-rich surface of the slag with 28 % Fe_2O_3 shown in Table 1 inhibits strong mechanical interlocking with the gypsum matrix. Consequently, this limited stress transfer displaying modest specific strength in the unmodified composite [7, 9]. In contrast, the GLS sample demonstrated a more pronounced enhancement in impact energy absorption compared to the control. This improvement is attributed to the chemisorption of stearic acid onto the CaO and alumina (Al_2O_3) sites of the slag surface. Consequently, the slag surface is expected to transform into an organophilic species. Thus, the fatty acid chains act as a micro-lubricant and a flexible interphase at the slag-gypsum boundary. Instead of a rigid, brittle connection. During mechanical loading the LS powder effectively hinders crack propagation and enhances the ability of the overall inorganic crystalline-amorphous framework to absorb sudden shock [20, 21]. The GN sample achieved the highest specific impact strength in the water binder series. The highest performance is a direct result of the high-aspect-ratio of the platy clay within the Nanofil-15. These platelets, modified with quaternary ammonium salts, are expected to promote electrostatic and hydrogen bonding interactions with the calcium-rich (CaO) hydration products of the gypsum. The platy morphology of the organoclay not only provides a high surface area for matrix reinforcement but also acts as a physical barrier that forces crack propagation along highly tortuous pathways. This synergistic effect i.e. Combining the localized lubrication provided by the platy shape of the Nanofil-15 together with the physical crack-path modification of the silicate layers. Such synergism provides a toughening efficiency that exceeds that of the GLS. In conclusion, the impact performance hierarchy for the water bound system is as:

GN > GLS > GS > G.

UP-bound system

The impact of utilizing UP as a binder is detailed in Table 3. The specific strength increased profoundly with the incorporation of the UP matrix for all prepared samples. Note that the UPG formulation displays the highest impact resistance compared to other formulas. This dramatic enhancement implies that the UP binder significantly improves the interfacial bonding between the fine gypsum particles and the UP phase. The plausible explanation to this enhancement is attributed to ligand-to-metal coordination between the nucleophilic groups (carbonyl of ester) of the UP resin and the electrophilic Ca^{2+} and Al^{3+} surface cations of mineral powder. This chemical coupling effectively bridges the amorphous silicate network of the slag and the crystalline sulfate lattice of the gypsum, facilitating a dense and cohesive

Table 3. Specific impact strength of binder-free and UP-bound gypsum hybrids reinforced with steel slag and organo-nanoclay.

Formula	Density, g cm^{-3}	Impact energy, J	Impact strength, kJ m^{-2}	Specific impact strength, kJ cm^3 m^{-2} g^{-1}
G	2.31	0.04	1.33	0.58
GS	2.5	0.03	1	0.4
GLS	2.41	0.06	2	0.83
GN	2.31	0.09	3	1.3
UPG	2.11	0.8	26.67	12.64
UGS	2.27	0.4	13.33	5.87
UGLS	2.2	0.25	8.33	3.79
UGN	2.12	0.12	4	1.89

interfacial transition zone. Such zone resists deformation and inhibits crack propagation. Provided that the strong interaction results in encapsulating the inorganic precursors by the UP resin creates a robust, continuous matrix that successfully bridges the amorphous (slag) and crystalline phases (gypsum), providing the primary mechanism for high-energy shock absorption i.e. specific impact strength.

Flexural performance

The flexural strength of the water-bound series estimated using Eq. (3) follows a clear hierarchy, as illustrated in Fig. 1: GN > GLS > GS > G. In this system, strength is primarily governed by the hydration of the crystalline gypsum lattice and the physical interlocking of the fillers. The higher performance of the GN and GLS samples suggests that organic modifications improve the homogeneity within the gypsum matrix. The flexural strength of the UP-bound hybrids is presented in Fig. 2. The results indicate that the replacement of the water-binding phase with the 10 % UP binder significantly enhanced flexural strength across all formulations. This improvement is a consequence of superior stress transfer facilitated by coordination forces at the UP-filler interface as mentioned earlier between electron donors (carbonyl groups of UP) and the electron-accepting Ca^{2+} and Al^{3+} cations on the surfaces of the gypsum and slag. This robust chemical adhesion effectively stiffens the composite under flexural loading. interestingly, UPN sample maintained the highest values. This should be attributed to the high-aspect-ratio of the platy nano silicate and their ability to form dense coordination networks with the resin. Ultimately, the conclusion is that the performance of the UP-bound system is governed by synergistic two factors, the former is the coordination-driven binding capacity of the polyester resin, and the latter is the structural reinforcement provided by the filler geometry.

Water absorption and porosity relationship

The moisture resistance profile for the gypsum hybrids, as a function of filler type and binder system is calculated according to Eq. (5), is summarized in

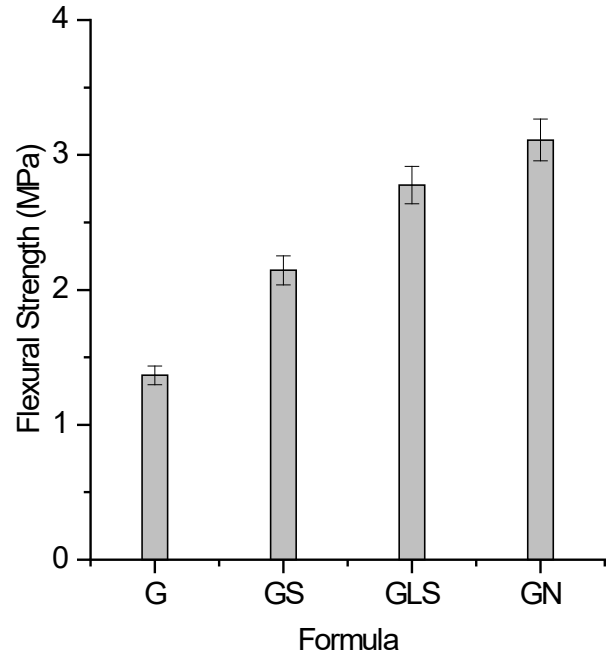

Fig. 1. Flexural strength of various gypsum hybrids.

Table 4. Theoretical density (ρ_{th}), experimental density (ρ_{exp}), degree of porosity (V), and water uptake percentages for the prepared composite formulations.

Symbol	ρ_{exp}	ρ_{th}	Porosity, Vv %	Water Uptake, M %
G	2.31	2.35	1.70	85
GS	2.5	2.56	2.34	80
GN	2.36	2.4	1.67	43
GLS	2.41	2.52	4.37	38
UPG	2.11	2.15	1.86	1.00
UPS	2.27	2.4	5.42	0.30
UPN	2.12	2.16	1.85	0.20

Table 4. For the water binder system, the water uptake capacity follows the rank: G > GS > GLS > GN. This behaviour is closely correlated with the degree of porosity (Vv) calculated for each formulation using Eq. (6). Note that the lower void volume generally restricts the capillary pathways available for transport. The GN composite exhibits a significant reduction in water uptake (~ 43 %) compared to the pure gypsum control (~ 85 %). This improvement is primarily driven by the unique geometry of the Nanofil-15 filler. The high-aspect-ratio, the morphology that effectively fills the interstitial gaps within the crystalline gypsum lattice. Consequently, this leads to denser packing and reduced porosity. Furthermore, these platelets act as impermeable obstacles, creating a tortuous path. Which forces water molecules to navigate a significantly longer and more complex path through the matrix. Notably, the GLS sample showed the lowest water uptake in the water binder series (~ 38 %), despite having a higher calculated porosity of 4.37 %. The stearic acid-treated slag (LS) utilizes a chemically hydrophobic barrier. The stearic acid molecules orient their polar heads toward the surface Ca^{2+} sites via coordination, while their hydrophobic tails reduce the surface energy of the pore walls, preventing capillary suction into the voids.

In the UP-bound system, water resistance is further enhanced as the 10 % UP binder provides a second level of protection. The polymer resin encapsulates the fillers, sealing the capillary pathways through coordination forces where the ester carbonyl groups act as ligands for the Ca^{2+} and Al^{3+} cations. The combination of the planar geometry of the clay provides physical barriers and the coordination-driven seal of the resin provides chemical barriers results in the exceptionally low uptake of 0.2 % seen in the UPN formulation.

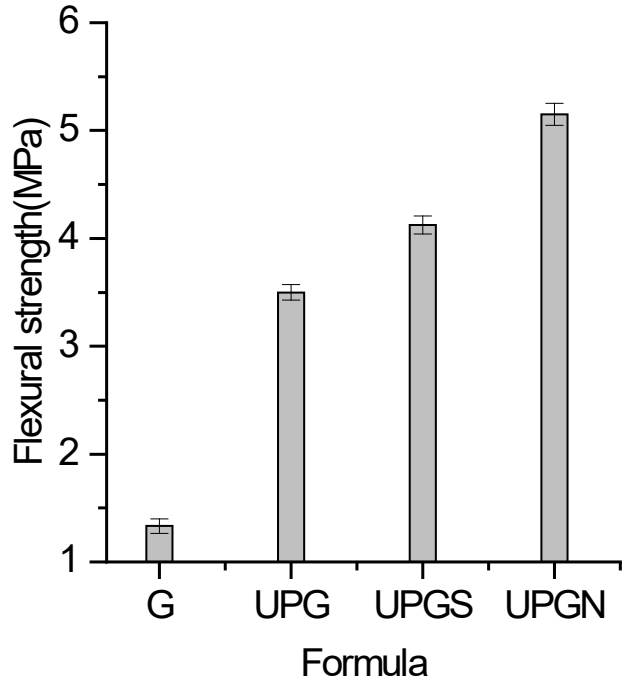

Fig 2. Flexural strength of various gypsum hybrids with UPE as binder.

Fire resistance of binder free and UP-bound hybrids

The resistance to direct flame exposure for both the water bound and UP-bound gypsum hybrids is summarized in Table 5, as determined by Eqs. (7) and (8), respectively. The ability to resist direct fire exposure is quantified through both percentage mass loss and the calculated M L R. For the binder-free system, fire resistance follows the rank of GS > GLS > GN > G. As shown in Table 5, the GS formula exhibited the highest thermal stability with the lowest mass loss of 13.4 % and a

Table 5. Comparative M % and MLR of gypsum hybrids under direct flame exposure for 0.5 min.

Formula	Initial mass, g	Weight loss, %	Mass loss Δm, g	MLR, g cm^{-2} s^{-1}
G	3	19.3	0.579	3.22×10^{-3}
GN	3	16.2	0.486	2.7×10^{-3}
GLS	3	14.2	0.426	2.37×10^{-3}
GS	3	13.4	0.402	2.23×10^{-3}
UP	3	67.8	2.034	11.3×10^{-3}
UPG	3	43.6	1.308	7.27×10^{-3}
UPN	3	39.8	1.194	6.63×10^{-3}
UPGLS	3	36.8	1.104	6.13×10^{-3}
UPGS	3	26	0.78	4.33×10^{-3}

corresponding MLR of 2.23×10^{-3} g cm^{-2} s^{-1}. Conversely, the G sample displayed the highest degradation as reflected by the loss of 19.3 % of its mass. This trend confirms that the incorporation of inorganic fillers significantly enhances the thermal resistance of the gypsum matrix. The superior performance of the slag-filled hybrids namely GS and the GLS should be attributed to the refractory nature of the steel slag. Due to the high concentrations of Al_2O_3 (13 %) and Fe_2O_3 (28 %) identified in the XRF data shown in Table 1. This allows the slag to act as an inorganic heat sink. These particles possess high thermal mass and emissivity, absorbing and dissipating thermal energy while moderating heat flow through the matrix. On the other hand, the GLS sample showed a slightly higher weight loss (14.2 %). This should be related to the thermal decomposition of the organics, namely stearic acid chains. Note that GLS remained significantly more resistant than the control (G). This indicates that the mechanical benefits of organic treatment come with only a minor thermal trade-off. The UP-bound system exhibited a marked increase in weight loss and MLR compared to the binder-free series. For instance, the UPG control lost 43.6 % of the original mass. This decrease in fire resistance is directly ascribed to the combustible organic nature of the UP binder. Recall that irrespective of the substantial mechanical advantages and structural integrity provided by the coordination forces between the UP resin and the surface Ca^{2+} and Al^{3+} ions, the carbon-rich polymer matrix remains the primary source of fuel during direct flame exposure. Thereby compromising less overall thermal stability compared to the purely (unmodified) inorganic filler.

Fracture topography

The SEM impact fractured surface of pure gypsum is shown in Fig. 3. The microstructure is characterized by brittle failure, featuring platy needle-like crystals that lack extensibility. Crack propagation occurs directly through the crystalline lattice with minimal diversion. This straight-line crack path and the absence of crack-bridging features explain the low impact energy absorption of G sample explained earlier. This observation is consistent with previous reports of unreinforced gypsum systems [22]. The impacted fracture SEM of the GS composite is presented in Fig. 4. The gypsum matrix and untreated slag appear irregular with insufficient interfacial bonding. Microcracks propagate linearly along the slag-matrix interface with minimal deviation. This behaviour confirms the structural dissimilarities and weak stress transfer

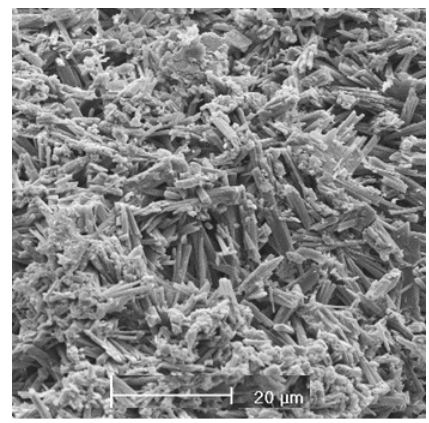

Fig. 3. SEM image of surface fractured G composite.

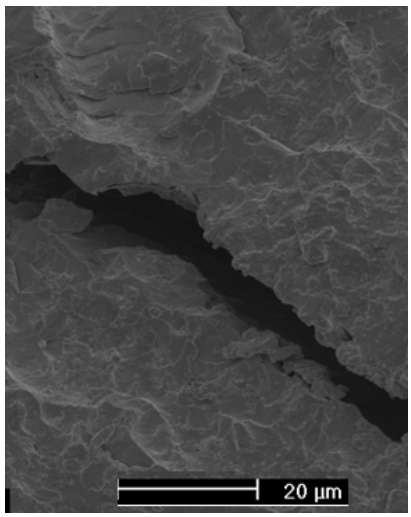

Fig. 4. SEM image of the fractured surface of GS hybrids.

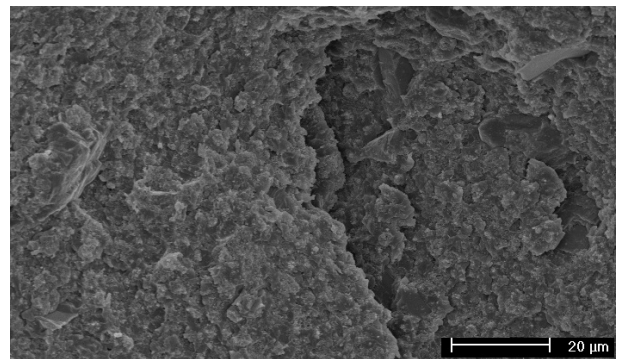

Fig. 5. SEM image of surface fractured GLS hybrid.

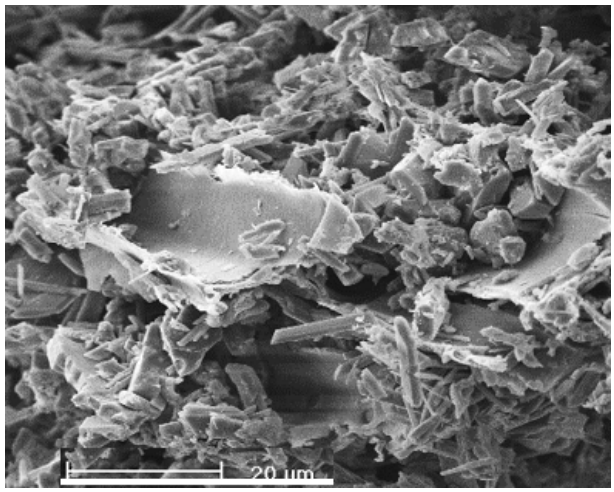

Fig. 6. SEM image of surface frectured GN hybrid.

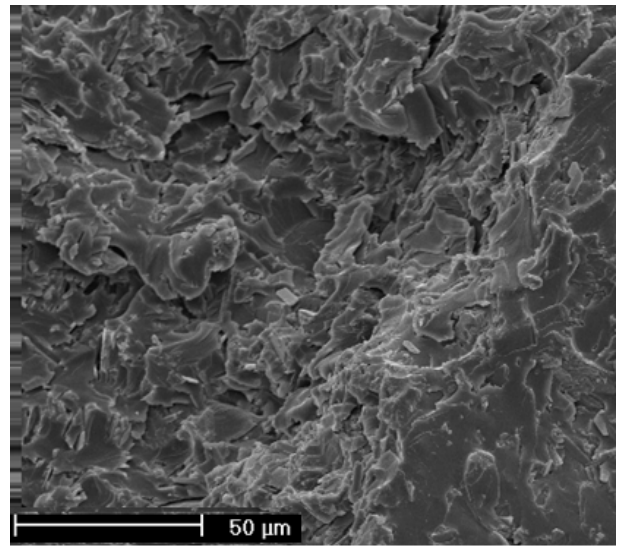

Fig. 7. SEM image of surface frectured UPG hybrid.

between the phases [8]. This microstructural evidence justifies the marginal reinforcement detected in the raw slag series. In contrast, the SEM micrographs of the GLS fractured surface shown in Fig. 5 reveal a higher degree of interaction between the modified slag and the gypsum. The structure is more consolidated, with fewer voids and improved cohesion. This enhanced interfacial cohesion is triggered by the chemisorption of stearic acid after modification. This is expected to reduce crack-initiation sites and promotes resistance to brittle fracture. This might explain the better energy absorption of the lubricated slag compared to G and GS counterparts. The SEM image of the GN fractured surface presented in Fig. 6 provides direct evidence of the plate-like Nanofil-15 structures. The nanoclay is uniformly distributed within the gypsum matrix. In this regard the high-aspect-ratio platelets force cracks to follow tortuous pathways. This geometric obstruction increases the energy required for fracture and improves overall impact toughness [4]. For the UP polymer-bound system, the SEM observations are summarized in Fig. 7. The fractured surface of the UPG composite shows a well-wetted interface with less void content. This morphology is indicative of cohesive fracture within the polymer matrix. This suggests that

the coordination forces between the resin and the surface ions elaborated earlier were strong. Where failure occurs primarily through the resin rather than at the filler interface. This topography stands to explain the high impact resistance recorded for the UP series. These findings align with reported features for UP/gypsum hybrids, where robust resin-filler interactions - driven by durable chemical and secondary bonding-correlate with enhanced impact properties.

CONCLUSIONS

This study developed and characterized two gypsum-based composite systems utilizing industrial steel slag and organo-nanoclay. The key findings are:

- In the binder-free system, mechanical performance improved in order: GN > GLS > GS > G. The GN formulation provided the highest specific impact and flexural strength due to the high-aspect-ratio silicate platelets which enhance crack-path tortuosity and nano-scale reinforcement.
- The GLS system outperformed raw slag (GS) because stearic acid chemisorption onto CaO and Al_2O_3 surface sites act as a flexible interphase that facilitates energy dissipation under load.
- The UP-bound system produced substantial increase in mechanical toughness. This enhancement is attributed to coordination interaction between the polyester carbonyl groups and the surface cations of the inorganic fillers.
- While the polymer binder provides mechanical advantages, it reduced fir resistance due to its combustible nature. Conversely, the binder-free GS formulation maintained better thermal stability, benefiting from the high Fe_2O_3 and Al_2O_3 content of the slag as an efficient inorganic heat sink.
- Water uptake was lowest in the nanoclay-filled samples due to reduced Vv and geometric diffusion barriers. The GLS sample demonstrated that hydrophobic surface modification can suppress moisture absorption even when void volume is relatively high.
- The UP-bound system achieved near-zero water absorption (< 1%), confirming that the polymer matrix successfully encapsulates hydrophilic mineral particles and provides hydrophobic barrier.

Acknowledgment

The author acknowledges department of materials Engineering of Al-Balqa Applied University-Jordan for the lab facilities.

Authors' contributions

The author was responsible for the experimental design, data analysis and preparation of the manuscript.

REFERENCES

1. S. Attia-Essaies, N. Barhoumi, H. Ayachi, H. Bouraoui, F. Srasra, Thermal and Mechanical Performances of Unsaturated Polyester Composites Reinforced by Natural Fillers, Chem. Afr., 7, 2024, 1523-1533.
2. Z. Li, Y. Zhang, X. Cao, J. Li, Y. Yuan, Preparation and Properties of Composite Cementitious Material Based on Steel Slag, Coal-Fired Slag, and Desulfurization Gypsum, Coatings, 15, 2025, 1280.
3. A. Mousa, G. Heinrich, U. Wagenknecht. Bio-Based Fillers. In: Kobayashi, S., Müllen, K. (eds), Encyclopedia of Polymeric Nanomaterials, Springer, Berlin, Heidelberg, 2014, 1-4.
4. Z. Bantie, A. Tezera, D. Abera, T. Nega, Nanoclays as Fillers for Performance Enhancement in Building and Construction Industries, IntechOpen, London, 2024, 1-14.
5. M. Keppert, R. Černý, A. Vimmrová, Investigation of gypsum composites with different lightweight fillers, Constr. Build. Mater., 297, 2021, 1-11.
6. A. Mousa, U. Wagenknecht, M. Gedan-Smolka, Cure Characteristics and Thermal Behavior of Organic–Inorganic Hybrid Composite as Assessed by DSC, TGA, and DMA Techniques, J. Sustain. Metall., 5, 2019, 442-448.
7. Y. Zhao, J. Qiu, Z. Ma, Temperature-dependent rheological, mechanical and hydration properties of cement paste blended with iron tailings, Powder Technol., 381, 2021, 82-91.
8. X. Zhang, X. Yang, J. Yang , S. Yin, W. Bian, Y. Qi, Development of magnesium slag-steel slag-based composite cementitious material and its backfilling application, Arch. Civil Mech. Eng., 25, 2025,194-208.

9. S. Cao, GL. Xue, E. Yilmaz, ZY Yin, FD. Yang, Utilizing concrete pillars as an environmental mining practice in under-ground mines, J. Clean. Prod., 278, 2021, 1-15.
10. S.M.S. Al-Mufti, A. Almontasser, S.J.A. Rizvi, Unsaturated Polyester Resin Filled with Cementitious Materials: A Comprehensive Study of Filler Loading Impact on Mechanical Properties, Microstructure, and Water Absorption, ACS Omega, 8, 2023, 20389-20403.
11. S. Cao, G. Xue, W. Song, Q. Teng, Strain rate effect on dynamic mechanical properties and microstructure of cemented tailings composites, Constr. Build. Mater., 247, 2020, 1-14.
12. A. Mousa, G. Heinrich, U. Wagenknecht, Toughened Unsaturated Polyester Composites Reinforced with Slag Material, Polym. Plast. Technol. Eng., 56, 2017, 1657-1664.
13. A. Mousa, M. Gedan-Smolka, K. Schlenstedt, Preparation and Characterization of Slag Reinforced Toughened Epoxy Composites, J. Chem. Technol. Metall., 60, 2025, 113-120.
14. A. Mousa, The Effect of Feldspar and Kaoline on Mechanical performance of SBR/LDPE composites, Int. J. Ind. Chem., 4, 2013, 26-34.
15. M. Bhong, T.K. Khan, K. Devade, B.V. Krishna, S. Sura, H.K. Eftikhaar, H.P. Thethi, N. Gupta, Review of composite materials and applications, Mater. Today: Proc., 77, 2023, 321-326.
16. A. Mousa, U.S. Ishiaku, Z.A.M. Ishak, Dynamic vulcanisation of poly (vinyl chloride)-epoxidised natural rubber thermoplastic elastomers, Plast. Rubber Compos. Process. Appl., 26, 1997, 331-335.
17. S. Akkoyun, Mechanical properties and interfacial interactions in oleyl titanate-treated blast furnace slag/polypropylene composites, J. Appl. Polym. Sci., 139, 2022, 1-11.
18. J. Li, S.Q. Zhang, Q. Wang, W. Ni, K.O. Li, P.F. Fu, W.T Hu, Z.F Li, Feasibility of using fly ash-slag-based binder for mine backfilling and its associated leaching risks, J. Hazard. Mater., 400, 2020,1-12.
19. A. Mousa, M. Gedan-Smolka, U. Wagenknecht, activated slag as an additive to rubberized unsaturated polyester composite: Thermal and mechanical study, J. Chem. Technol. Metall., 55, 2020, 173-179.
20. A. Mousa, Cure Characteristics and Thermal Properties of Sulfur-Cured EPDM-Based Composites by Compounding with Layered Nano-Organoclays. Polym.-Plast. Technol. Eng., 45, 2006, 911-915.
21. A. Mousa, M. Gedan-Smolka, Modification of Mineral Powder by Various Organic Materials: Their Potential as Reinforcement for Unsaturated Polyester Composites, Russ. J. Appl. Chem., 93, 2020,1968-1975.
22. A. Souidi, M. Atigui , Y. Maaloufa, M. Amazal, S. Oubeddou, S. Mounir, A. Aharoune A, Comparative Study of Gypsum Composite Materials Reinforced with Date Palm and Polyester Fibres, J. Compos. Advanc. Mater., 34, 2024, 133-142.